Mapping and Monitoring Of Water Hyacinth In Lake Victoria Using Polarimetric Radar Data

Isundwa K. Felix, *Student Member, IEEE,* Marino Armando, *Member, IEEE,* Morgan David Simpson, Akbari Vahid, *Member, IEEE,* Thiago S. F. Silva, Aviraj Datta, Prabhu G. Nagendra, Gogumalla Pranuthi, Rupavatharam Srikanth

***Abstract*—Water hyacinth, an invasive species originating from South America, has become a significant concern since its introduction in Lake Victoria (Kenya), particularly in the Winam Gulf, where large annual blooms are observed. Monitoring the occurrence and location using in situ methods is expensive and challenging due to the lake's vastness. Remote sensing monitoring methods offer an alternate option due to the ability to cover vast areas. This study explores the potential of polarimetric Synthetic Aperture Radar (PolSAR), specifically utilising Sentinel-1 VV-VH data to map and monitor water hyacinth cover. The change detection method based on Optimisation of Power Difference (OPDiff) and minimum eigenvalue selection achieves a remarkable accuracy of 98.89% in separating clear and water hyacinth-infested water. Using polarimetric data offered better separability, enabling spatial and temporal monitoring. The analysis reveals that in 2018 water hyacinth cover peaked, spanning over 200 km^2. Temporal variability showcases a seasonal rise and peak from September to December. This research demonstrates the capability of using PolSAR data to accurately map and monitor water hyacinth's spatial and temporal dynamics, offering valuable insights for effective management strategies.**

***Index Terms*—SAR polarimetry, optimisation of power difference, water hyacinth monitoring, and change detection.**

I. Introduction

This article presents a methodology for the detection and monitoring of an invasive aquatic plant, water hyacinth (WH), using polarimetric SAR (PolSAR) data from the ESA Sentinel-1 satellites. Water hyacinth is the common name given to plants from the genus *Pontederia* (formerly *Eichhornia*), especially the species *Pontederia crassipes*[1]. WH originates from tropical South America and has a high potential to become invasive. A single WH plant is capable of producing up to 14 x 10^7 'daughter' plants in a year [2], which will occupy an area of approximately 1.4 Km^2. WH has been identified among the most dangerous invasive species by the International Union for Conservation of Nature (IUCN) due to its adverse socio-economic impacts and difficulty in elimination from water bodies [3]. WH can cause severe effects on the environment where it blooms, such as increasing the incidence of malaria & filariasis, decreasing fish populations, hampering recreation and navigation, and sometimes clogging dams [2], [4]. The decay of WH can deposit approximately 1000 metric tons in wet weight per hectare per year [5].

Isundwa K. F. is a student at the University of Stirling, Stirling, FK9 4LA, Scotland, UK. (e-mail: f.k.isundwa@stir.ac.uk).

Manuscript received March 20, 2024; revised April 28, 2024 and September 9, 2024.

WH was introduced to Lake Victoria in 1889 and established itself by spreading along the shores of the lake. It is still spreading one hundred years after its introduction, where it has been seen to form mats that cover more than 70 square miles [6]. WH has been traditionally monitored in Lake Victoria through anecdotal accounts, rough estimates, and local field observation in the 1990s and early 2000s[7]. These measurements are limited in coverage, labour intensive, time-consuming, and expensive [8]. Field surveys are also hampered by the amount of data collected, leading to a limited understanding of the factors that influence the dynamics of WH [9].

Remote sensing offers a less expensive alternative for monitoring WH [10]. It has been shown that remote sensing provides the capability to distinguish and quantify WH infestation from a colour infrared imagery from multiple sites [11], and mapping of WH at a large scale has been demonstrated using optical data from Landsat-8 [12]. The mapping of aquatic plants using Landsat, ENVISAT/MERIS[13], TERRA/ASTER and field measurements have also been demonstrated before[14]. Normalised difference vegetation index (NDVI) from Sentinel-2 was used to monitor WH and Chl-a in Lake Tana in Ethiopia [15]. However, cloud coverage remains a potential challenge to continuous and all-weather monitoring when using optical data, especially in regions with long rainy seasons or high cloud cover.

Synthetic aperture radar (SAR) imagery can be collected at any time of day and almost independently of weather conditions, thus offering varied applications [16]. A SAR-based remote sensing approach was utilised to classify aquatic plants along the Amazon floodplain, mapping their cover and estimating net primary productivity [17]. Previous classification of vegetation in wetland areas, including aquatic plants, has achieved producers' accuracy of over 85% using SAR data [18], [19], and the use of SAR L-band data in estimating above-ground biomass resulted in promising spatial and quantitative outputs for the Amazon floodplains [20], [21]. The accuracy of above-ground biomass estimation is dependent on vegetation morphology, the type and size of vegetation, and different phenological stages, which will interact with the radar frequency used and with surface conditions to determine the contribution of varying scattering mechanisms [22], [23]. Zhou [24] found that the combination of backscattering coefficients and polarimetric decomposition components from Sentinel-1 SAR data significantly improved wetland classification accuracy. Similarly, RADARSAT2 polarimetric data was used to

map surface water and flooded vegetation areas ([25]. The potential of ALOS PALSAR dual-polarimetric (dual-pol) in detecting water level changes and flow patterns in wetland environments was further demonstrated [26]. These studies have demonstrated the effectiveness of dual-pol SAR in detecting and classifying features in water bodies and wetlands.

Full-polarimetric (quad-pol) PolSAR data is needed to fully characterise surface scattering mechanisms. However, access to this data type is minimal due to availability, cost and low-frequency repeat cycles, preventing time series analysis. Conversely, dual-polarimetric data is accessible and freely available, and, in the case of Sentinel-1, it offers a 6 to 12-day repeat cycle within the existing historical record (2015 to present). Our research thus explores the polarimetric capabilities of dual-pol imagery. Due to this, our research explores the polarimetric capabilities of dual-pol and its application to water body monitoring by trying to answer the question, "Can the Optimisation of the Power Difference method successfully quantify WH cover in Lake Victoria?". To answer this question, we sought the following specific objectives:

1) To separate WH-infested waters from clear waters using dual-pol SAR polarimetry.
2) To quantify the spatial and temporal trends of WH in Lake Victoria.
3) To identify the areas with high incidence of WH coverage between 2017 and 2022.

II. MATERIALS AND METHODS

A. Study Area

Our study area is Winam Gulf, a section of Lake Victoria which covers most of the shoreline of the Republic of Kenya (Africa, Fig. 1). Kisumu City, Kenya's third largest city, is within the shores of Winam Gulf, and other major urban centres in the region include Kendu Bay and Homa Bay. Rivers Nyando, Awach Kano, Sondu-Miriu, Awach Seme, Nyamasaria, Awach Kibwon and several other seasonal rivers drain into Winam Gulf. These rivers drain watersheds with mixed land use activities ranging from highly agricultural to urban to forested areas [27].

B. Data

In this work, we used dual-polarimetric (dual-pol) data acquired by the Sentinel-1 constellation of the EU Copernicus programme, provided by the European Space Agency (ESA) [29]. To maximise the polarimetric information, we used Interferometric Wide Single Look Complex (IW SLC) data with a 5m by 20m spatial resolution [29]. The SLC image is a level-1 product containing focused SAR data that has been geo-referenced using orbit and altitude information from the satellite and is provided in slant-range geometry. Corrections have been made to the elevation antenna pattern, range spreading loss, and azimuth bi-static delay. SLC images contain VV and VH channels, where V stands for vertical linear polarisation, and H stands for horizontal linear polarisation. The temporal resolution of the data is 12 days for a single satellite and six days between the two satellites, Sentinel-1 A (S1A) and Sentinel-1 B (S1B). In total, 438 individual

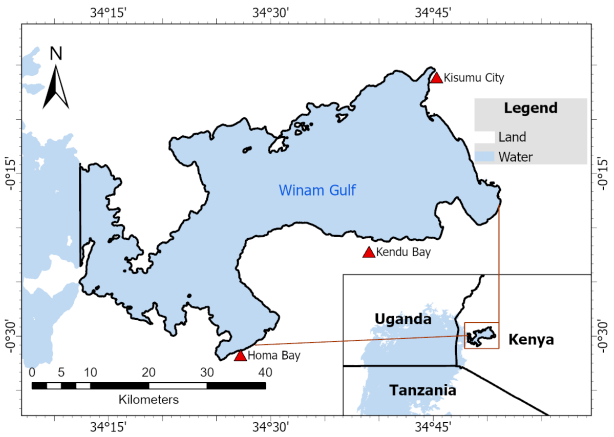

Fig. 1. Map of the Winam Gulf area of Lake Victoria, Kenya. The map shows the outline of the Winam Gulf section of the lake about the larger section shared between Kenya, Uganda and Tanzania. Shoreline data from Hamilton, Stuart, 2016 [28]

images were analysed for the period between January 2017 to November 2022. The satellite passes over the Winam Gulf differed in coverage Fig. 2, with no pass fully covering the Gulf. For this reason, each satellite pass was analysed separately and herein referred to as a frame. Frame 1 (track-130), frame 2 (track-50) and frame 3 (track-28) were all acquired at different periods, spatial coverage, and in both ascending and descending orbits (Table I). Although frames partially overlap, the high variability in WH cover due to wind required us to analyse each frame separately instead of mosaicking.

C. Scattering Model

Open surface waters will be seen as 'solid' when considering scattering mechanisms, as the radar signal does not penetrate liquid water and is scattered away from the antenna. Depending on wind conditions, two backscattering scenarios are possible. If surface waters are calm, and have minimal roughness, we expect specular scattering (mirror-like). This type of scattering often occurs in lakes during low wind conditions. In this situation, most signals are scattered away from the sensor, leading to very dark image tones that enable easy classification of open waters. As moderate to strong winds develop, capillary waves will be formed on the water surface, increasing the amount of backscattering (a Bragg Surface, [30]). The polarimetric behaviour of this surface scattering scenario results in co-polarised (VV) backscattering being much higher than cross-polarised (VH) backscattering.

When considering eigenvalue decomposition, a 'pure' target can be described by a single scattering matrix when only one eigenvalue is nonzero. In such a case, the covariance or coherence matrix will have a rank equal to 1. This rank also applies to a spatially extended scatterer with one single scattering mechanism. On the other hand, if all the eigenvalues are nonzero and approximately equal, the covariance or coherence matrix has orthogonal scattering mechanisms from non-polarised random scattering structures. As vegetation causes random volume scattering, it will result in a rank

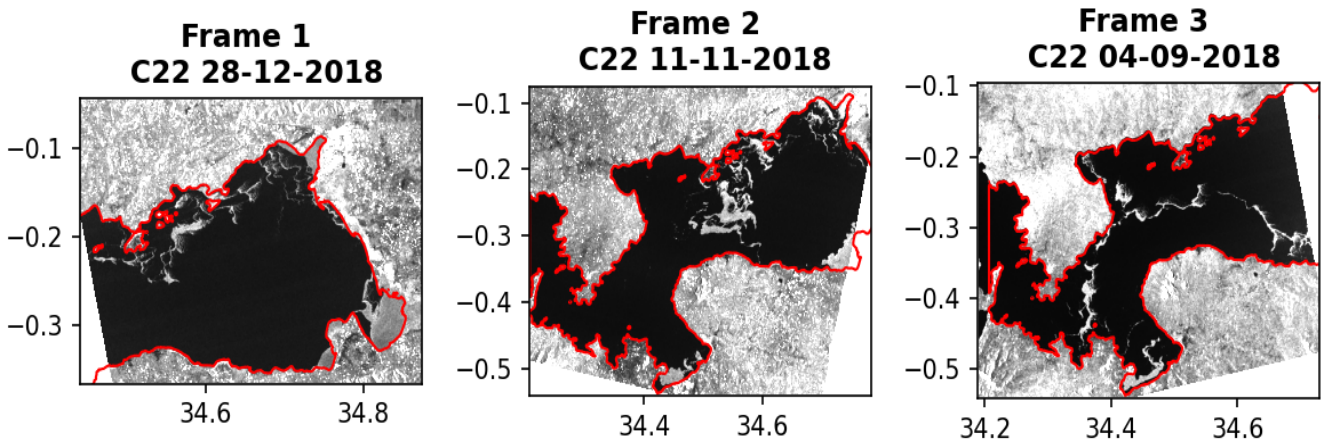

Fig. 2. Plot of the 3 Sentinel-1 frames covering Winam Gulf, Lake Victoria, Kenya. Frame 1 adequately covers the eastern section of the lake while missing the western side. Frame 2 covers most of the gulf except a section in the east. Frame 3 covers the western and central sections but misses the eastern sections. The plots represent the C22 elements of the covariance matrix with contrast-enhanced by a factor of 2.

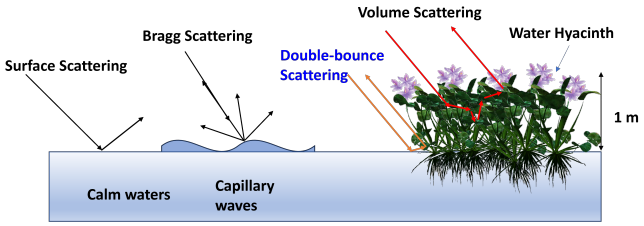

Fig. 3. The figure of scattering occurring on the lake's surface. Surface scattering from calm waters (left), Bragg scattering from capillary waves(centre) and depolarisation from the volume of WH on the surface of the lake (right).

higher than rank 1 [31]. A model can be used to separate the different scattering mechanisms in fully polarimetric data. Still, a specific model can not be used in this study because of the data available. Therefore, in this study, volume scattering is referred to as the depolarisation effect from the volume of WH, which can grow and reach up to 1m on the surface of the water [32]. It is clear, therefore, how PolSAR can help discriminate between increased surface scattering (produced by waves) and depolarisation by volume of WH (made by vegetation), as shown in Fig. 3. Research established that in wetlands, where water is beneath the vegetation surface, double-bounce scattering occurs in instances where the vegetation is sparsely spaced, and the signal penetrates past the vegetation canopy. This is mainly due to slanting vegetation, modelled as oriented targets (including dihedrals) [33]. A similar scattering mechanism may occur with WH. The double-bounce scattering has been established to be spread in cross-pol channels in SAR data. Therefore, WH's double-bounce and volume scattering contribution will be spread in the co- and cross-pol channels. This is consistent with other findings that double-bounce scattering dominates scattering from wetlands [34].

It is important to note that emergent floating vegetation on top of the water would trigger volume scattering. Therefore, it is impossible to discriminate WH from other aquatic plants without using additional ancillary information. However, for the case of Lake Victoria, WH has been previously observed during field measurements as the only floating vegetation that colonises open waters, with only minimal and opportunistic occurrence of hippo-grass and papyrus plants[7].

D. PolSAR Processing

Our methodology has four main processing steps: pre-processing, co-registration, change detection, and thresholding. The ESA SNAP Graph Processing Tool (GPT) was used to execute the first two steps using batch processing. The change detection and thresholding steps are performed afterwards.

The SLC files contain amplitude and phase information of the electromagnetic wave [35]. During the pre-processing steps, the scattering vector in the data is used to calculate the polarimetric covariance matrix, which is used in further processing [36]. While the polarisation state of single scatterers can be deterministically described using a scattering matrix, distributed partial targets require a stochastic description of the scattering mechanism using a coherency or covariance matrix. The dual-pol covariance matrix includes the multi-look intensities of co-polarisation VV, cross-polarisation VH, and their cross-correlation VV*VH.

The covariance matrix extracted for each pixel then enables the use of eigen-decomposition to obtain eigenvalues and eigenvectors that describe scattering characteristics [37] and allow separation of the contribution of scattering mechanisms (eigenvalues) and the type of scattering mechanisms (eigenvectors) [31]. To separate clear and WH-infested waters, optimal descriptors of land cover must be determined. To understand the separability between clear and WH-infested

waters, backscatter intensities and polarimetric descriptors of pixels were analysed for sample ROIs using scatter plots. Backscattering coefficient values in VV and VH on the dB scale were examined. At the same time, for polarimetric data, eigenvalues from the eigenvalue decomposition of the polarimetric covariance matrix (Cloude-Potier decomposition) and the change matrix (OpDiff) were conducted.

E. Water Hyacinth Detection Algorithm

The change detection method of Optimisation of Power Difference (OPDiff) was applied in this study [38]. This method is preferred due to its capability to quantify both the magnitude and the direction of change. For that, the covariance matrices from *date1* and *date2* are subtracted to produce the Change Matrix. The optimisation of this matrix then allows us to extract the scattering mechanisms that suffered the maximum or minimum change, where an additive model (OPDiff) of change is exploited. Therefore, after the optimisation, the largest eigenvalue (if the value is positive) represents the power of the largest scattering mechanism added to a scene. The minimum eigenvalue (if negative) is the power of the scattering mechanism that was maximally removed from the scene. Conversely, minimum vectors will represent scattering mechanisms which have been removed while the maximum eigenvectors will represent the scattering mechanisms added [38], [39]. The advantage of optimisation is that the SM constantly changes, and this technique aligns with the one that changes the most. This is more robust than fixing the SM since, as in the case of WH, the resulting SM from WH's volume is unknown due to its randomness. As proposed by Marino [38], the change matrix can be found as shown in equation (1).

$$[C_c] = [C_{d1}] - [C_{d2}] \tag{1}$$

where $[C_c]$ is defined as **change matrix** a difference between two normal matrices, $[C_{d1}]$ is the covariance matrix from date of interest and $[C_{d2}]$ is the covariance matrix of the reference image. A step-by-step derivation of the formula is detailed in [38]. After obtaining the change matrix, the maximum and minimum eigenvectors and corresponding eigenvalues of this matrix are found by applying the Lagrangian optimisation, differentiation and diagonalisation (2) to obtain Lagrangian multipliers of $[C_c]$.

$$C_c\underline{\omega} = \lambda\underline{\omega} \tag{2}$$

$[C_c]$ is Hermitian, but it is not positive semi-definite. Therefore, it will have eigenvalues that are real but not necessarily positive. Since $[C_c]$ is normal, the set of eigenvectors are orthogonal and represent minimal change that can be applied additively to transform the first partial target into the second partial target. The scattering mechanisms are the same vector that forms the covariance matrix, and this is because the change matrix is a difference of two normal matrices, but they lose the property of semi-positive definiteness. The loss of definitiveness is because the intensity for a scattering mechanism can either increase or decrease in power [38]. If the absolute phase of the scattering mechanism changes, PolSAR will not be able to detect it, and you will need polarimetric interferometric SAR (PolInSAR). A change in the channels' phase will produce a change in the scattering mechanism, which PolSAR will detect.

In simpler terms, the OPDiff method finds a linear combination of polarimetric channels that provide the smallest or highest difference. The outputs of this are two eigenvalues λ_i and two eigenvectors u_i which represent the magnitude of change and the scattering mechanism that has changed, respectively. To detect WH, $[C_{d2}]$ (reference scene/image) is selected from a date when there was no WH. *Note: The reference image/scene is fixed and is subtracted from all other images*. In this context, the reference scene $[C_{d2}]$ will have only scattering from the lake surface and without WH, while the second scene $[C_{d1}]$ if WH is present will have scattering from the volume of WH. Thus, the change matrix $[C_c]$ will encapsulate scattering from the volume of WH added (surface scattering removed). The interest is thus a positive value from increased eigenvalues (SM added to the scene). Thresholding is applied to select positive values (scattering due to the volume of WH) while rejecting any removal of scattering power. This algorithm was previously tested and found to be the best performing by Simpson *et al*. [40], in Vembanad Lake in India. A fundamental difference is that unlike [40], where the maximum eigenvalues were considered, the minimum eigenvalue of the change matrices is used here. The difference is that Lake Victoria is a large lake, and winds can be high, creating a higher likelihood of strong surface scattering. Fortunately, as mentioned before, surface scattering is polarised (it is a single scattering mechanism) and will impact only the first eigenvalue. In contrast, the depolarised scattering from a volume of WH will spread over both eigenvalues. The change detector is, therefore, filtering out the increase in polarised scattering and detects only increases in unpolarised scattering or targets with a large entropy. For this reason, wind information is not considered part of the equation. Still, its impact is accounted for by considering unpolarised scattering and neglecting the increase in backscatter intensity due to wind (increase in polarised scattering). By not having quad-pol information available, there could be some ambiguity in defining the type of volume scattering. However, a random volume scattering in dual-pol will be visible as the second eigenvalue increases. In a practical sense, the minimum eigenvalue can reject false WH detection from Bragg/wave surface scattering, which is secluded to the first eigenvector.

Before applying the OPDiff detection methodology to extract WH, polarimetric filtering was applied using the Boxcar filter [41] with a 7 by 7 window. This window was revealed to be the best in our application. After change detection, a histogram plot was used to select an eigenvalue threshold separating clear and WH-infested water.

Each frame's images were used to create data cubes(here referred to as stacks) containing several images. A stack is a 3-dimensional array of pixels in range and azimuth direction, with the third dimension being when the individual image was acquired. Three different stacks were generated for the three frames. After change detection, a threshold was applied to individual images within each stack, resulting in binary images with 0 for clear water and 1 for WH. Each cube generated a separate frequency of occurrence map of WH for

TABLE I
SATELLITE IMAGERY FRAMES, ORBITS REFERENCE IMAGES AND PROCESSING TIME

Frame	No. of images	Reference image	Orbit direction	Processing time (hrs)
Frame 1	174	10/10/2017	Ascending	23
Frame 2	114	29/09/2017	Descending	13
Frame 3	150	03/10/2017	Ascending	21

each of the three frames. It is important to note that the three frames were analysed independently, producing three stacks. That is to say, each image within a stack was compared only to the reference extracted from the same stack. This ensures that residual backscattering differences caused by changes in incidence and look angles (not entirely removed by the terrain correction) do not produce comparison artefacts. The number of SLC acquisitions for each frame and reference images are shown in Table I.

F. Accuracy Assessment

Accuracy and validation of the selected threshold was done using ROI's generated from Planet Labs data [42]. Digitized polygons were generated from Planet Labs optical data in Fig. 4 and used for accuracy assessment. The optical data is available in Blue, green, red and Near Infrared bands with a resolution of 3 meters. A total of 1000 threshold values equally distributed between the minimum and maximum values were tested to optimise the classification threshold. For each threshold value selected, the probability of detection (PD) (true positive rate), probability of false alarm (PF) (false positive rate), precision, F1-score and accuracy were calculated as elaborated in equations 3-6 [43] .

$$\text{PD} = \frac{\text{True Positives}}{\text{True Positives + False Negatives}} \tag{3}$$

$$\text{PF} = \frac{\text{False Positives}}{\text{False Positives + True Negatives}} \tag{4}$$

$$\text{Precision} = \frac{\text{True Positives}}{\text{True Positives + False Positives}} \tag{5}$$

$$\text{F1-Score} = \frac{\text{False Positives}}{\text{False Positives + True Negatives}} \tag{6}$$

The calculated parameters were plotted and used together with a histogram plot to select the optimal threshold for separating WH for all frames. This was done using optical data acquired on 24-09-2018. Optical data acquired on 28-09-2018, 22-10-2018 and 15-02-2019 was later used for validation. The validation data from digitised ROIs had a total area of 3251.9 Ha of WH and 4722 clear water (391,081 pixels). All the optical datasets used in validation were acquired on the same day as Sentinel-1 data but with a few hours difference between them. The validation results are represented in table II. It is important to note that WH floating patches may move if there is a time difference between optical data and Sentinel-1 acquisition; therefore, a slight underestimation of accuracy is expected. Since all phenological stages occur throughout the year and our objective was to map WH cover density rather than phenological differences, using a single image to validate each frame was sufficient to assess the accuracy of detectors. The optical data used was of high resolution (3 meters) and, therefore, sufficient to visually separate clear and WH areas used in assessing the accuracy and validation. A negative buffer of 50m was applied on the boundaries of Lake Victoria. This buffer enabled the masking of land areas, the exclusion of water level changes, and human activity on the shoreline. All classification results were masked using this buffer.

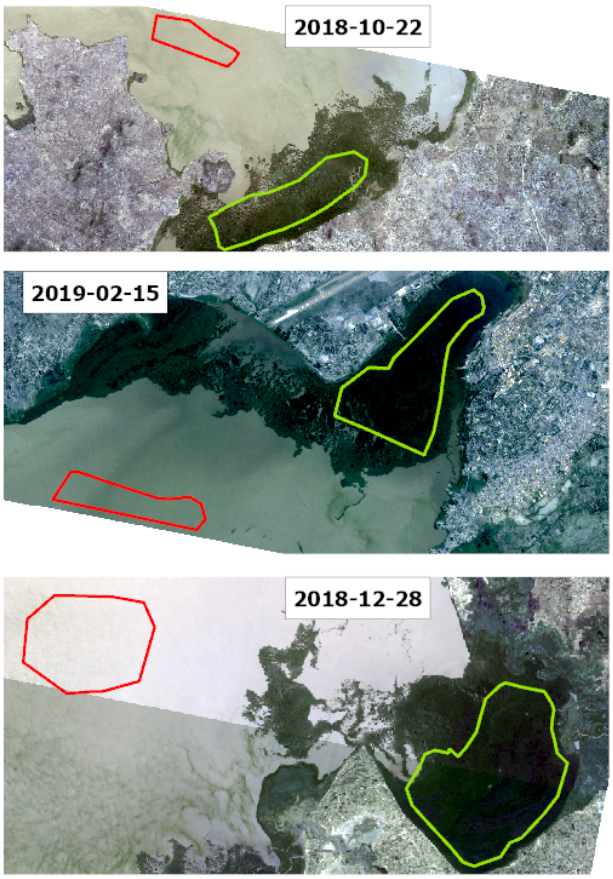

Fig. 4. The Plot of three Planet Labs optical data Scenes acquired on 2018-10-22, 2019-02-15, and 2018-12 were used to validate the change detection. The red outline shows digitised areas with no WH, while the green polygon shows the areas covered with WH. The blue outline is the lake shoreline. Image © 2024 Planet Labs PBC

III. RESULTS

A. Water Hyacinth and Clear Water Separability

The application of scatter plots in understanding the separability of WH from clear water demonstrated the advantages of utilising polarimetric data. Polarimetric data provides separability regardless of the conditions on the lake's surface. On a calm day, the backscattering coefficient values of WH and clear water in VV and VH polarisation in dB scales show overlap and high spread in both polarisations. This will, in principle, complicate the separation of WH and clear water. On a windy day, a different characteristic is observed. There

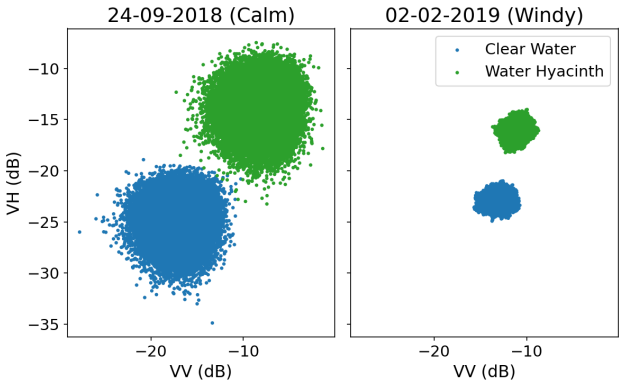

Fig. 5. Scatter plot of WH-infested and clear waters backscattering coefficient values plotted on dB scale for VH polarisation against VV polarisation. The Plot on the left was acquired on 24-09-2018 on a calm/low wind day, while the Plot on the right was acquired on 02-02-2019 on a windy day. The blue dots represent values of clear water pixels, while the green dots represent values of WH-infested waters. The number of pixels for each date used in generating the plots are 24-09-2018 (WH -64,860 & clear water-52,962) and 02-02-2019 (WH-9,775 & clear water-18,352).

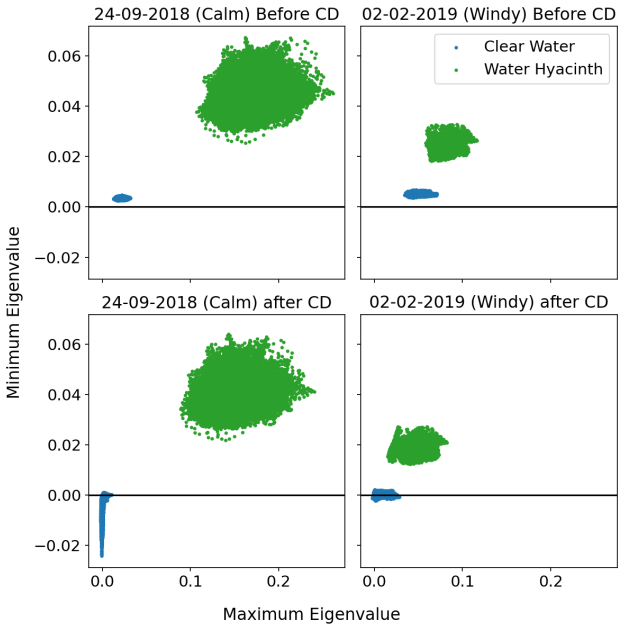

Fig. 6. The figure represents plots of minimum eigenvalues against maximum eigenvalues from the Cloude-Potier decomposition. The blue dots are values of clear water pixels, while the green dots are values of WH-infested water. The top-left is a plot of images acquired on 24-09-2018 (calm day) before change detection (raw eigenvalues). The bottom left is a plot after change detection. The image on the top-right is a plot of eigenvalues of data acquired on 02-02-2019 (windy day) before change detection. The image on the bottom right is a plot after change detection. The number of pixels for each date used in generating the plots are: 24-09-2018(WH-32,928 & clear water 26,578) and 02-02-2019 (WH-8,240 & clear water-4,860)

is a low spread of backscattering coefficient values on the VV and VH dB scales and observable overlap in VV polarisation, unlike in VH, where two distinct classes are visible. Therefore, there is better separability when VH backscattering coefficient data on a windy day, as shown in Fig. 5. The VV and VH backscattering values could not provide a single threshold separability for a calm and windy day. On a calm day, clear waters have a very low spread before applying change detection, while WH eigenvalues have a high spread. There is separability between WH and clear water in maximum and minimum eigenvalues. Similar characteristics are observed after performing change detection. On a windy day, however, the low spread is observed on both clear water and WH, but unlike on a calm day, separability is only observable on minimum eigenvalues. Maximum eigenvalues show overlap before and after change detection, as shown in Fig. 6. For this reason, the minimum eigenvalue was selected as the most robust metric for mapping WH regardless of lake surface conditions such as wind.

B. Accuracy Assessment and Validation

Inspecting of WH and clear water pixels over the lake showed a bimodal distribution in Fig. 7. This distribution enabled the selection of a threshold (0.005) to separate the two classes. This threshold was then adopted for all frames. This threshold was arrived at based on the histogram and accuracy assessment plot where the highest PD, accuracy and F1-score were recorded with the lowest PF as shown in Fig. 8. The threshold values between 0 and 0.02 had high detection accuracy for all frames. Threshold values below 0 had low accuracy and F1-score, with high PD and PF. Between the intervals, there is the highest PD, accuracy and F1 score and PF lowest. Beyond this threshold interval, the PD, PF, F1-score and accuracy drop to the lowest values. Therefore, the optimum threshold applicable for selecting WH-

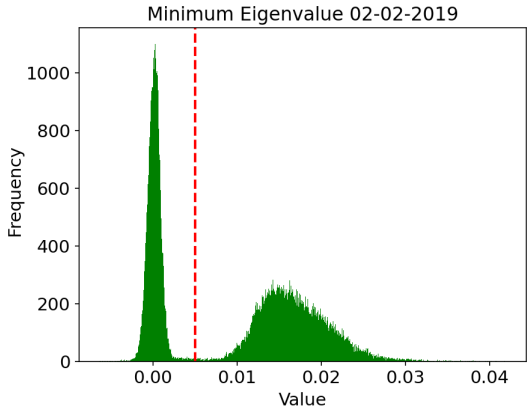

Fig. 7. Histogram of the minimum eigenvalue of WH and clear water on a windy day. The red vertical line shows the value of the threshold (0.005) that was applied to separate the two classes of WH and clear water. The left side of the line represents the distribution of the clear water pixels, while the right side represents the distribution of WH pixels.

infested waters is between the two threshold intervals. Thus, the decision was made to choose 0.005 as the threshold.

C. Water Hyacinth Coverage Maps

The application of the detector in separating the floating vegetation from the clear water demonstrates the capability to detect floating vegetation. Visual inspection of the VV polarisation intensity data shows brighter areas over the lake

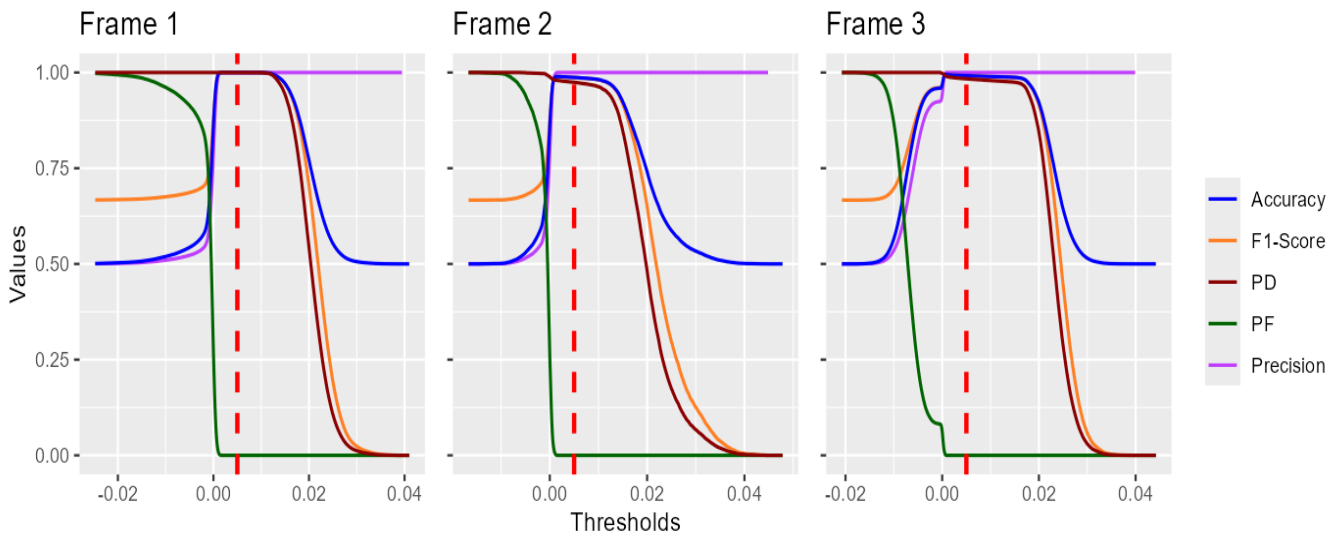

Fig. 8. The Plot of the probability of detection (PD), probability of false alarm (PF), accuracy, and F1-score against the thresholds selected. The red vertical dashed line shows the adopted threshold (0.005) for all the frames.

TABLE II
A TABLE OF VALIDATION OF CHANGE DETECTION FOR EACH FRAME. THE TABLE WHEN THE ACCURACY WAS ASSESSED USING PLANET LABS DATA ACQUIRED ON THE SAME DAY AS SENTINEL-1 DATA ACQUISITION.

Frame	Date	Probability of detection/recall	Probability of false alarm	Accuracy	F1-score
1	2018-12-28	0.99992	0.0	0.99996	0.99996
2	2019-02-15	0.97434	0.0	0.98717	0.98700
3	2018-10-22	0.98351	0.0	0.99175	0.99168

surface when WH is present versus dark areas on days without WH presence. After performing change detection and applying the threshold of minimum eigenvalues, areas with no visible floating vegetation on VV polarisation record no WH over the lake based on eigenvalues. On dates where floating vegetation is observable on the VV polarisation, WH is detected and isolated from surrounding clear waters Fig. 9.

D. Spatial and Temporal Variability in Water Hyacinth cover

There is significant variability in the movement of WH across the lake. Evidence of temporal change in WH area coverage is observable over time with movements in both east to west & west to east directions, mainly due to wind action over the lake. This spatial variability is observable in the entire Winam Gulf or when focusing on a Gulf section shown in Fig. 10 over 25 days. Since the detector was accurate in separating clear and WH-infested waters, it also enabled the estimation of the area covered by WH on each day of Sentinel-1 acquisition. A time series of the area covered by WH for the different frames was generated, showing the monthly, seasonal and annual WH variability during the study period. 2018 recorded the largest area extent covered by WH in the period between 2017 and 2022 with an area of over 200 km^2 as shown in Fig. 11.

The generated WH coverage maps enabled quantifying how frequently WH occurred over the gulf. The frequency of

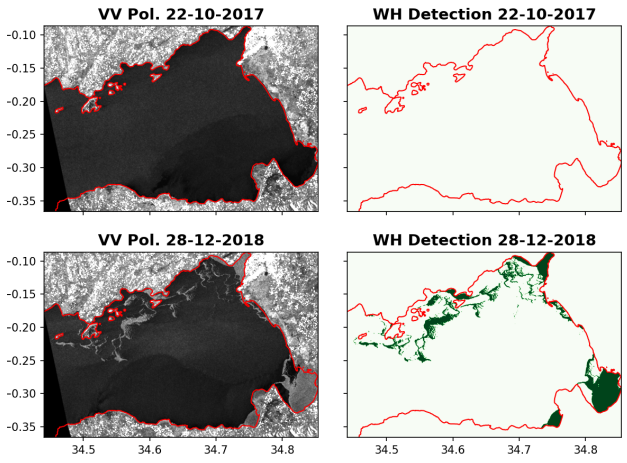

Fig. 9. Plot of SAR images acquired and analysed to detect WH. The top left shows the VV polarisation channel image acquired on 22-10-2017 with no WH on the lake's surface. After change detection, the top right shows no WH on the lake's surface. The bottom left shows the VV polarisation image acquired when WH was present in the lake on 28-12-2018. The bottom right tile shows the presence of WH on the lake's surface, which is represented by dark green features within the red outline of the lake on 28-12-2018. The red outline represents the lake shoreline. **Note:** the axes units are degree decimal for latitude and longitudes

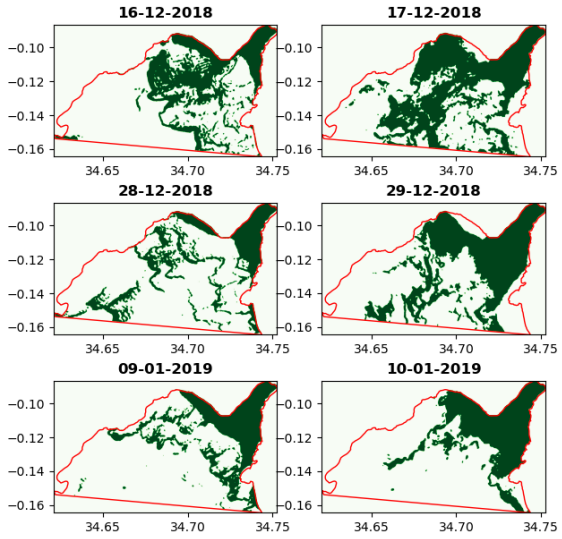

Fig. 10. The tile showing WH detection in the Kisumu area between 16-12-2018 and 10-01-2019 shows spatial variability. The dark green patches represent the detected WH in the section of the lake. The red outline represents the lake shoreline manually snapped to cover the Kisumu area only to aid visual interpretation. **Note:** the axes units are degree decimal for latitude and longitudes

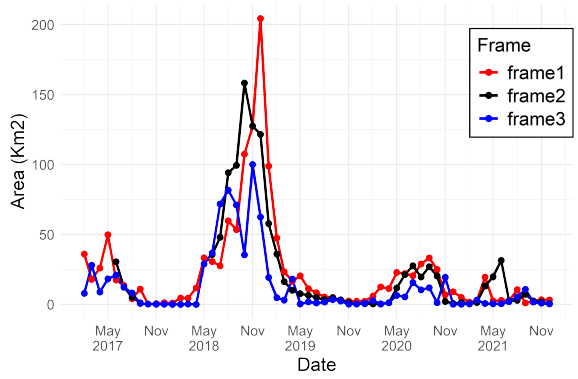

Fig. 11. Time series plot of the monthly maximum area in square kilometres of WH coverage for the three frames.

occurrence map generated for each frame identified that during the analysis period, some sections of the lake recorded WH presence up to 30% of the time (Fig. 12), while the Kisumu area to the Northeast recorded WH for up to 20% of the time. The high spatial and temporal variability of WH cover was evident from the frequency of occurrence map, where WH cover was recorded at least once in almost all sections of the lake.

IV. Discussion

Using dual-pol data to detect and monitor WH has shown great potential with highly accurate detection. The polarimetric decomposition of SLC data into eigenvalues improved the separability of water hyacinth and clear water, enabling using a single threshold under different wind conditions. This separability would otherwise be complex when using backscattering coefficients only. The minimum eigenvalue provided better separability of classes due to its ability to detect unpolarised scattering while filtering out the increase in polarised scattering. This finding is similar to previous research [40] where the use of optimisation of additive polarimetric changes demonstrated capabilities to separate floating vegetation and lake wave scattering. Unlike [40], where the maximum eigenvalues were considered, we found that using minimum eigenvalues better captured WH changes. Besides monitoring floating vegetation, using SAR data may thus enable the separation of emergent floating plants such as WH from algal blooms, which would be challenging using optical data [44]. Dual-pol data enables the separation of different scattering mechanisms occurring in a scene and, in this case, allows detection of the scattering mechanism added in a scene (depolarisation by volume of WH) when compared against surface scattering (when there was no WH). The application of the OPDiff methodology shows great potential in monitoring aquatic emergent vegetation on a single image or in a time series.

Our method allowed us to consistently quantify WH cover area over time and demonstrate the high degree of spatial and temporal variability of WH distribution in Lake Victoria. The frequency of WH over the lake shows that WH was present at some point in almost all sections of the lake, but some areas are particularly susceptible to clogging by WH. The Kisumu area, for example, an essential area for water transport in Lake Victoria, has recorded clogging 20% of the time. As our goal in this study was to optimise the WH detection method, we have not investigated the causes of seasonal increase and decrease in spatial coverage, and further understanding should be sought to assess which elements influence WH cover. Still, we expect our method to help researchers to quantify and track these patterns over time. Considering the findings, the methodology demonstrates the potential of applicability in different lakes and regions. The methodology can be applied regardless of the wind condition since minimum eigenvalue filters out polarised scattering while detecting unpolarised scattering from WH. However, applying the method in a different environment should select a threshold suited for the region. Future research will focus on automated threshold selection.

V. Conclusion

This article presents a methodology to map and monitor spatial and temporal variability of Water Hyacinth (*Pontederia* spp.) using dual-pol SAR data from the Sentinel-1 satellites. The OPDiff change detection approach was applied to identify the scattering mechanisms that suffer maximum and minimum change between observations. Our detector accurately separated calm and rough open water from WH-infested water, allowing regular spatial and temporal variability monitoring. Our method allowed us to establish which areas experience Water Hyacinth clogging most often and the duration and timing of these events. We also demonstrated the high mobility of Water Hyacinth mats, as almost all areas of the lake surface

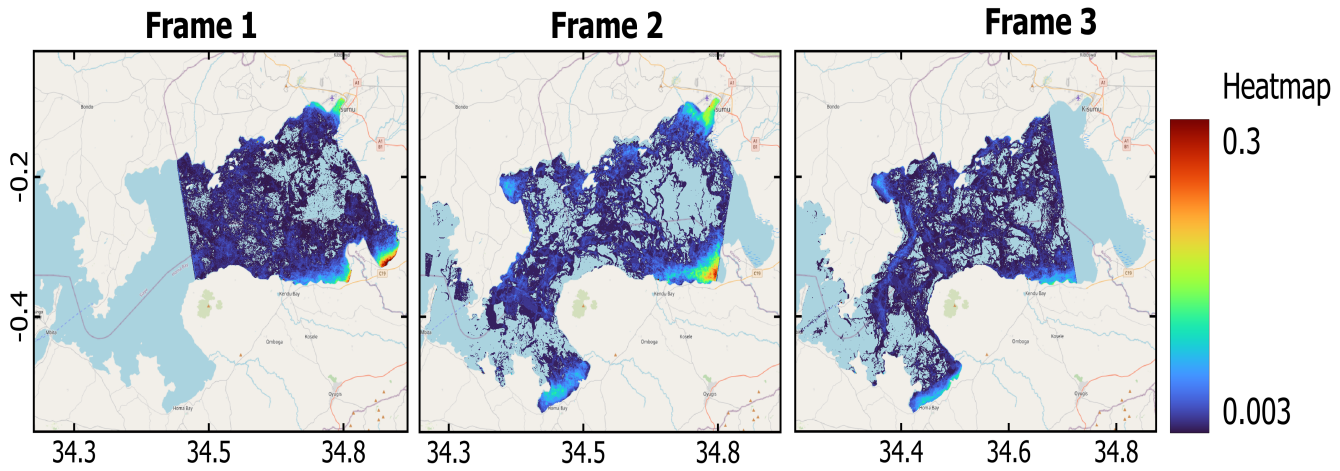

Fig. 12. The heat maps generated for the three frames also show the coverage of the gulf. The heat map shows values ranging from 0 to 0.3, where 0 represents pixels that did not record any WH presence from the data/dates analysed, while 0.3 represents the presence of WH in 30% of the data/images analysed per frame. **Note:** the axes units are degree decimal for latitude and longitudes

recorded the presence at least once. Additional research is needed to understand how temporal variability of climate and water quality influences Water Hyacinth distribution in Lake Victoria.

VI. Acknowledgment

The UKRI Global Challenges Research Fund supported this work through a grant (F\1920\1\37) from the Royal Academy of Engineering. The work also received support from the Biotechnology and Biological Sciences Research Council [grant number BB\X511985\1]. Sentinel-1 data is provided courtesy of the European Space Agency Copernicus Programme. PlanetScope high-resolution images were provided by Planet Labs PBC through the Education and Research Standard program. This work was also supported by the Natural Environment Research Council via an IAPETUS2 PhD studentship held by Isundwa Kasiti Felix (grant reference NE/S007431/1).

References

[1] A. M. Villamagna and B. R. Murphy, "Ecological and socio-economic impacts of invasive water hyacinth (Eichhornia crassipes): a review," *Freshwater biology*, vol. 55, no. 2, pp. 282–298, 2010.

[2] G. K. Gaurav, T. Mehmood, L. Cheng, J. J. Klemeš, and D. K. Shrivastava, "Water hyacinth as a biomass: A review," *Journal of Cleaner Production*, vol. 277, p. 122214, 2020. [Online]. Available: https://www.sciencedirect.com/science/article/pii/S0959652620322617

[3] T. R. Téllez, E. M. d. R. López, G. L. Granado, E. A. Pérez, R. M. López, and J. M. S. Guzmán, "The water hyacinth, Eichhornia crassipes: An invasive plant in the Guadiana River Basin (Spain)," *Aquatic Invasions*, vol. 3, no. 1, pp. 42–53, 2008.

[4] T. J. Stohlgren, P. Pyšek, J. Kartesz, M. Nishino, A. Pauchard, M. Winter, J. Pino, D. M. Richardson, J. Wilson, B. R. Murray, M. L. Phillips, L. Celesti-Grapow, and J. Graham, "Globalization effects on common plant species," in *Encyclopedia of Biodiversity (Second Edition)*, S. A. Levin, Ed. Waltham: Academic Press, 2013, pp. 700–706. [Online]. Available: https://www.sciencedirect.com/science/article/pii/B9780123847195002392

[5] D. Simberloff, "Introduced species, impacts and distribution of," in *Encyclopedia of Biodiversity (Second Edition)*, S. A. Levin, Ed. Waltham: Academic Press, 2013, pp. 357–368. [Online]. Available: https://www.sciencedirect.com/science/article/pii/B9780123847195002513

[6] N. W. Wawire and G. R. S. Ochiel, "Review of the impact of water hyacinth on Lake Victoria : the case of," 1996.

[7] T. Albright, T. Moorhouse, and A. Mcnabb, "The rise and fall of water hyacinth in Lake Victoria and the Kagera River Basin, 1989-2001," *J. Aquat. Plant Manage*, vol. 42, pp. 73–84, jul 2004.

[8] J. H. Ritchie, Jerry C. and Zimba, Paul V. and Everitt, "Remote Sensing Techniques to Assess Water Quality," *Photogrammetric Engineering & Remote Sensing*, vol. 69, no. 6, 2003.

[9] A. Datta, S. Maharaj, G. N. Prabhu, D. Bhowmik, A. Marino, V. Akbari, S. Rupavatharam, J. A. R. P. Sujeetha, G. G. Anantrao, V. K. Poduvattil, S. Kumar, and A. Kleczkowski, "Monitoring the Spread of Water Hyacinth (Pontederia crassipes): Challenges and Future Developments ," 2021. [Online]. Available: https://www.frontiersin.org/articles/10.3389/fevo.2021.631338

[10] J. H. Everitt, C. Yang, D. E. Escobar, C. F. Webster, R. I. Lonard, and M. R. Davis, "Using Remote Sensing and Spatial Information Technologies to Detect and Map Two Aquatic Macrophytes," *Journal of Aquatic Plant Management*, vol. 37, no. 2, pp. 71–80, 1999. [Online]. Available: http://hdl.handle.net/1834/19622 https://aquadocs.org/bitstream/1834/19622/1/v37p71.pdf

[11] R. L. Shilpakar, J. X. Li, L. Ge, P. Dawson, and S. Chapman, "Water hyacinth mapping in gwydir wetlands using remote sensing techniques," in *19th NSW Biennial Weeds Conference Papers Experience the Highs–working smarter together*, 2017.

[12] R. M. Cavalli, G. Laneve, L. Fusilli, S. Pignatti, and F. Santini, "Remote sensing water observation for supporting Lake Victoria weed management," *Journal of Environmental Management*, vol. 90, no. 7, pp. 2199–2211, 2009.

[13] E. K. Cheruiyot, C. Mito, M. Menenti, B. Gorte, R. Koenders, and N. Akdim, "Evaluating MERIS-Based Aquatic Vegetation Mapping in Lake Victoria," pp. 7762–7782, 2014.

[14] F. Mancini, M. De Giglio, and M. Nurra, "Use of Landsat and Terra-ASTER data for environmental monitoring," *Italian Journal of Remote Sensing*, vol. 40, pp. 39–53, oct 2008.

[15] T. Mucheye, S. Haro, S. Papaspyrou, and I. Caballero, "Water Quality and Water Hyacinth Monitoring with the Sentinel-2A/B Satellites in Lake Tana (Ethiopia)," *Remote Sensing*, vol. 14, no. 19, 2022. [Online]. Available: https://www.mdpi.com/2072-4292/14/19/4921

[16] B. Brisco, "Early Applications of Remote Sensing for Mapping Wetlands," in *Remote Sensing of Wetlands*, mar 2015, pp. 86–97.

[17] T. S. F. Silva, M. P. F. Costa, and J. M. Melack, "Spatial and temporal variability of macrophyte cover and productivity in the eastern

Amazon floodplain: A remote sensing approach," *Remote Sensing of Environment*, vol. 114, no. 9, pp. 1998–2010, 2010. [Online]. Available: https://www.sciencedirect.com/science/article/pii/S0034425710001203

[18] R. Torres, P. Snoeij, D. Geudtner, D. Bibby, M. Davidson, E. Attema, P. Potin, B. Ö. Rommen, N. Floury, M. Brown, I. N. Traver, P. Deghaye, B. Duesmann, B. Rosich, N. Miranda, C. Bruno, M. L'Abbate, R. Croci, A. Pietropaolo, M. Huchler, and F. Rostan, "GMES Sentinel-1 mission," *Remote Sensing of Environment*, vol. 120, pp. 9–24, 2012. [Online]. Available: https://www.sciencedirect.com/science/article/pii/S0034425712000600

[19] V. Akbari, M. Simpson, S. Maharaj, A. Marino, D. Bhowmik, G. N. Prabhu, S. Rupavatharam, A. Datta, A. Kleczkowski, and J. A. R. P. Sujeetha, "Monitoring Aquatic Weeds in Indian Wetlands Using Multi-temporal Remote Sensing Data with Machine Learning Techniques," in *2021 IEEE International Geoscience and Remote Sensing Symposium IGARSS*, 2021, pp. 6847–6850.

[20] M. Costa, "Estimate of net primary productivity of aquatic vegetation of the Amazon floodplain using Radarsat and JERS-1," *International Journal of Remote Sensing*, vol. 26, no. 20, pp. 4527–4536, oct 2005. [Online]. Available: https://doi.org/10.1080/01431160500213433

[21] L. R. Sartori, N. N. Imai, J. C. Mura, E. M. L. d. M. Novo, and T. S. F. Silva, "Mapping Macrophyte Species in the Amazon Floodplain Wetlands Using Fully Polarimetric ALOS/PALSAR Data," *IEEE Transactions on Geoscience and Remote Sensing*, vol. 49, no. 12, pp. 4717–4728, 2011.

[22] C. Chen, Y. He, J. Zhang, D. Xu, D. Han, Y. Liao, L. Luo, C. Teng, and T. Yin, "Estimation of Above-Ground Biomass for Pinus densata Using Multi-Source Time Series in Shangri-La Considering Seasonal Effects," *Forests*, vol. 14, no. 9, 2023. [Online]. Available: https://www.mdpi.com/1999-4907/14/9/1747

[23] L. Tian, X. Wu, Y. Tao, M. Li, C. Qian, L. Liao, and W. Fu, "Review of Remote Sensing-Based Methods for Forest Aboveground Biomass Estimation: Progress, Challenges, and Prospects," *Forests*, vol. 14, no. 6, 2023. [Online]. Available: https://www.mdpi.com/1999-4907/14/6/1086

[24] G. Zhou, Z. Wang, H. Miao, C. Jiang, and G. Jing, "Wetland Classification in Poyang Lake Using Dual-polarization Synthetic Aperture Radar Data with Feature Combination," *Sensors and Materials*, 2021. [Online]. Available: https://api.semanticscholar.org/CorpusID:245536259

[25] W. Zhang, B. Hu, and G. Brown, "WETLAND CLASSIFICATION FOR BLACK DUCK HABITAT MANAGEMENT USING COMBINED POLARIMETRIC RADARSAT 2 AND SPOT IMAGERY," *The International Archives of the Photogrammetry, Remote Sensing and Spatial Information Sciences*, vol. XLII-3, pp. 2303–2306, 2018. [Online]. Available: https://isprs-archives.copernicus.org/articles/XLII-3/2303/2018/

[26] S. W. Kim, S. H. Hong, and S. Wdowinski, "Wetland monitoring using ALOS dual-pol SAR interferometry," in *2011 3rd International Asia-Pacific Conference on Synthetic Aperture Radar (APSAR)*, 2011, pp. 1–2.

[27] O. Masongo, P. Mwirigi, J. Okungu, J. Osio, J. O. Z. Abuodha, and R. E. Hecky, "Sedimentation in the Lake Victoria catchment and the Winam Gulf." 2005. [Online]. Available: https://aquadocs.org/bitstream/1834/7141/1/ktf0097.pdf http://hdl.handle.net/1834/7141

[28] S. A. N. S. F. Hamilton, "Shoreline, Lake Victoria, vector polygon, ∼2015." [Online]. Available: https://doi.org/10.7910/DVN/PWFW26

[29] Copernicus, "Copernicus sentinel data 2022. retrieved from asf daac 10/11/2022 processed by esa." Copernicus, 2015.

[30] L. L. Hess, J. M. Melack, A. G. Affonso, C. Barbosa, M. Gastil-Buhl, and E. M. Novo, "Wetlands of the Lowland Amazon Basin: Extent, Vegetative Cover, and Dual-season Inundated Area as Mapped with JERS-1 Synthetic Aperture Radar," *Wetlands*, vol. 35, no. 4, pp. 745–756, 2015.

[31] J.-S. Lee and E. Pottier, *Polarimetric Radar Imaging: From Basics to Applications*, 1st ed. Boca Raton: CRC Press, 2009.

[32] T. D. Center and N. R. Spencer, "The phenology and growth of water hyacinth (Eichhornia crassipes (Mart.) Solms) in a eutrophic north-central Florida lake," *Aquatic Botany*, vol. 10, pp. 1–32, 1981. [Online]. Available: https://www.sciencedirect.com/science/article/pii/0304377081900024

[33] S. H. Hong and S. Wdowinski, "Double-Bounce Component in Cross-Polarimetric SAR From a New Scattering Target Decomposition," *IEEE Transactions on Geoscience and Remote Sensing*, vol. 52, no. 6, pp. 3039–3051, 2014.

[34] B. Brisco, F. Ahern, S. H. Hong, S. Wdowinski, K. Murnaghan, L. White, and D. K. Atwood, "Polarimetric Decompositions of Temperate Wetlands at C-Band," *IEEE Journal of Selected Topics in Applied Earth Observations and Remote Sensing*, vol. 8, no. 7, pp. 3585–3594, 2015.

[35] R. K. Raney, H. Runge, R. Bamler, I. G. Cumming, and F. H. Wong, "Precision SAR processing using chirp scaling," *IEEE Transactions on Geoscience and Remote Sensing*, vol. 32, no. 4, pp. 786–799, 1994.

[36] D. Mandal, D. S. Vaka, N. Bhogapurapu, V. S. K. Vanama, V. Kumar, Y. Rao, and A. Bhattacharya, "Sentinel-1 SLC Preprocessing Workflow for Polarimetric Applications: A Generic Practice for Generating Dual-pol Covariance Matrix Elements in SNAP S-1 Toolbox," *Environmental Science, Engineering*, 2019.

[37] S. R. Cloude and E. Pottier, "A review of target decomposition theorems in radar polarimetry," *IEEE Transactions on Geoscience and Remote Sensing*, vol. 34, no. 2, pp. 498–518, 1996.

[38] A. Marino and M. Nannini, "Signal Models for Changes in Polarimetric SAR Data," *IEEE Transactions on Geoscience and Remote Sensing*, vol. 60, pp. 1–18, 2022.

[39] A. Marino and A. Alonso-Gonzalez, "Optimisations for different change models with polarimetric SAR," in *EUSAR 2018; 12th European Conference on Synthetic Aperture Radar*, 2018, pp. 1–5.

[40] M. D. Simpson, V. Akbari, A. Marino, G. N. Prabhu, D. Bhowmik, S. Rupavatharam, A. Datta, A. Kleczkowski, J. A. R. Sujeetha, G. G. Anantrao, V. K. Poduvattil, S. Kumar, S. Maharaj, and P. D. Hunter, "Detecting Water Hyacinth Infestation in Kuttanad, India, Using Dual-Pol Sentinel-1 SAR Imagery," *Remote Sensing*, vol. 14, no. 12, 2022. [Online]. Available: https://www.mdpi.com/2072-4292/14/12/2845

[41] A. J. Roscoe and S. M. Blair, "Choice and properties of adaptive and tunable digital boxcar (moving average) filters for power systems and other signal processing applications," in *2016 IEEE International Workshop on Applied Measurements for Power Systems (AMPS)*. IEEE, 2016, pp. 1–6.

[42] P. L. PBC, "Planet application program interface: In space for life on earth," Planet, 2018–. [Online]. Available: https://api.planet.com

[43] T. Fawcett, "Introduction to ROC analysis," *Pattern Recognition Letters*, vol. 27, pp. 861–874, jun 2006.

[44] D. Xu, Y. Pu, M. Zhu, Z. Luan, and K. Shi, "Automatic Detection of Algal Blooms Using Sentinel-2 MSI and Landsat OLI Images," *IEEE Journal of Selected Topics in Applied Earth Observations and Remote Sensing*, vol. 14, pp. 8497–8511, 2021.

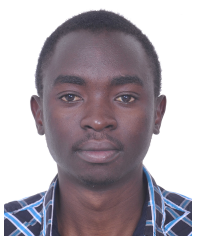

Isundwa Kasiti Felix (Student Member, IEEE) received his B.Sc. degree in Earth Sciences (Hydrology and Water Resources Management option) from Maseno University, Kenya in 2013. He worked as a consulting hydrologist from 2014 to 2016 and started his M.Sc. Degree. In 2018, he obtained his M.Sc. in Water Policy from the Pan African University Institute of Water and Energy Sciences (PAUWES). He later joined SERVIR Eastern and Southern Africa project at the Regional Centre for Mapping of Resources for Development, Nairobi, Kenya in 2019 as an assistant hydrologist. Since October 2022, he has been undertaking his PhD research in mapping and monitoring floods using SAR Polarimetry at the University of Stirling, Faculty of Natural Sciences, Stirling, UK.

Armando Marino (Member, IEEE) received the M.Sc. degree in telecommunication engineering from the Universita' di Napoli "Federico II", Naples, Italy, in 2006. In 2006, he joined the High Frequency and Radar Systems Department, German Aerospace Centre, Oberpfaffenhofen, Germany, where he developed his M.Sc. thesis. He received a PhD. in polarimetric SAR interferometry from the School of Geosciences, University of Edinburgh, Edinburgh, U.K. in 2011. From March 2011 to October 2011, he was with the University of Alicante, Institute of Computing Research, Spain. From December 2011 to May 2015, he was a Postdoctoral Researcher and Lecturer with ETH Zurich, Institute of Environmental Engineering, Switzerland. From June 2015, he was a Lecturer with the School of Engineering and Innovation, Open University, Milton Keynes, U.K. Since May 2018 he has been an Associate Professor at the University of Stirling, Faculty of Natural Sciences, Stirling, UK.

Morgan Simpson (Student Member, IEEE) received his B.Sc degree in Environmental Geography in 2019 from the University of Stirling, Scotland. He then obtained his M.Sc degree in Earth and Planetary Observation in 2020 from the University of Stirling. Since October 2020, he has been undertaking his PhD research in the remote sensing of marine plastics using radar data at the University of Stirling, Faculty of Natural Sciences, Stirling, UK.

Vahid Akbari received the Ph. degree in physics with a specialisation in radar remote sensing and data analytics from the UiT—The Arctic University of Norway, Tromsø, Norway, in 2013.

Since 2014, he continued his research in radar remote sensing and machine learning as a Postdoctoral Research Fellow with the UiT—The Arctic University of Norway, the Norwegian Institute of Bioeconomy Research, Akershus, Norway, and the University of Stirling, Stirling, U.K. He was a Visiting Scientist with Signal Processing and Telecommunications Laboratory, Department of Electrical, Electronic, Telecommunications Engineering and Naval Architecture, University of Genoa, Genoa, Italy, in 2011, and a Visiting Researcher with the German Geoscience Centre (GFZ), Potsdam, Germany, in 2008. He was an Assistant Professor at the University of Tehran in 2015. Since 2023, he has been a Lecturer (Assistant Professor) in data science/artificial intelligence with the University of Stirling. His primary research interests revolve around the intersection of radar remote sensing and statistical modelling/machine learning, with a particular focus on the applications in environmental monitoring

Thiago S. F. Silva received his BSc. in Biology from University of Rio Grande do Norte (UFRN, Brazil) in 2002, his M.Sc. degree in Remote Sensing from the National Institute for Space Research (INPE, Brazil) in 2004, and his PhD in Physical Geography from University of Victoria (Canada) in 2009. He worked then as a researcher at the University of California Santa Barbara in 2010 and INPE from 2011 to 2013. He then joined the Geography Department of São Paulo State University (UNESP) as an Assistant Professor from 2013 to 2019. Since 2019, he has been a Senior Lecturer at the University of Stirling, Faculty of Natural Sciences, UK. Dr. Silva's research combines ecology, geoscience and data science to understand how global ecosystems are being affected by the global climatic and biodiversity crises.